Neuro-Oncology 15(8):1027–1040, 2013.
doi:10.1093/neuonc/not046
Advance Access publication April 17, 2013

Molecular interactions of ErbB1 (EGFR) and integrin-β1 in astrocytoma frozen sections predict clinical outcome and correlate with Akt-mediated in vitro radioresistance

Miklós Petrás, Tamás Lajtos, Elza Friedländer, Álmos Klekner, Éva Pintye, Burt G. Feuerstein, János Szöllősi, and György Vereb

Department of Biophysics and Cell Biology (M.P., T.L., E.F., J.S., G.V.); Department of Neurosurgery (Á.K.); Department of Radiotherapy (É.P.); MTA Cell Biology and Signaling Research Group (J.S., G.V.), Medical and Health Science Center, University of Debrecen, Debrecen, Hungary; and Department of Neurology, Barrow Neurological Institute–St. Joseph's Hospital and Medical Center, University of Arizona College of Medicine, Phoenix, Arizona (B.G.F.)

Introduction. Treatment of astrocytoma is frequently hampered by radioresistance of the tumor. In addition to overexpression of ErbB1/EGFR, functional crosstalk between receptor tyrosine kinases and cell adhesion molecules may also contribute to therapy resistance.
Methods. Acceptor photobleaching FRET was implemented on frozen sections of clinical astrocytoma to check the role of ErbB1–integrin-β1 interaction. U251 glioma subclones were obtained by introducing extra CHR7 material or the ErbB1 gene to test the relevance and mechanism of this interaction in vitro.
Results. Grade IV tumors showed higher ErbB1 and integrin-β1 expression and greater ErbB1–integrin-β1 heteroassociation than did grade II tumors. Of these, the extent of molecular association was a single determinant of tumor grade and prognosis in stepwise logistic regression. In vitro, integrin-β1 was upregulated, and radiosensitivity was diminished by ectopic ErbB1 expression. Great excess of ErbB1 provided colony forming advantage over medium excess but did not yield better radiation resistance or faster proliferation and decreased to medium level over time, whereas integrin-β1 levels remained elevated and defined the extent of radioresistance. Increased expression of ErbB1 and integrin-β1 was paralleled by decreasing ErbB1 homoassociation and increasing ErbB1–integrin-β1 heteroassociation. Microscopic two-sided FRET revealed that pixels with higher ErbB1–integrin-β1 heteroassociation exhibited lowed ErbB1 homoassociation, indicating competition for association partners among these molecules. Boosted Akt phosphorylation response to EGF accompanied this shift toward heteroassociation, and the consequentially increased radioresistance could be reverted by inhibiting PI3K.
Conclusion. The clinically relevant ErbB1–integrin-β1 heteroassociation may be used as a target of both predictive diagnostics and molecular therapy.

Keywords: Akt-dependent radioresistance, astrocytoma fresh frozen sections, ErbB1 (EGFR), integrin-β1, molecular interaction predicting prognosis.

Tumors of the central nervous system are the second most frequent cause of cancer-related mortality among patients aged <35 years.[1,2] Of these tumors, high-grade astrocytomas show particularly bad prognosis. The actual therapeutic strategy for glial tumors consists of surgical resection as complete as achievable and treatment of the remaining tumor with adjuvant radio- and/or chemotherapy. Despite significant advances in neuroimaging, surgical technique, and adjuvant therapy over the past 50 years, malignant glioma remains a highly invasive and virtually incurable disease, of which treatment efficacy is frequently hampered by the decreased chemo- and radiosensitivity of the tumor cells.[3]

To date, several resistance mechanisms to irradiation have been proposed; however, underlying molecular interactions remain elusive. In addition to impaired DNA

Received December 4, 2012; accepted March 1, 2013.

Corresponding Author: György Vereb, MD, PhD, DSc, Department of Biophysics and Cell Biology, University of Debrecen MHSC, P.O. Box 39, H-4012 Debrecen, Hungary (vereb@med.unideb.hu).

damage checkpoint responses, disregulated signaling starting from assemblies of cell surface molecules, including growth factor receptors, has been also shown to play an important role. In this respect, members of the ErbB family of transmembrane receptor tyrosine kinases have been studied extensively.[4] ErbB1 (also known as EGFR or HER1) amplifications and mutations have long been recognized as common gain-of-function perturbations in malignant gliomas. ErbB receptor tyrosine kinases appear to participate in the response and resistance of tumor cells to ionizing radiation;[5] increased expression of ErbB1 correlates with decreased radiosensitivity in high-grade astrocytoma cells.[6] Furthermore, it has been revealed that tumor cells may express multiple ErbB family members, which can homo- and heteroassociate during signal transduction, leading to versatile downstream signaling events.[7] The balance between cytoprotective and cytotoxic responses to ErbB1 activation during single and repeated radiation exposures has been shown to depend on the relative expression levels and activities of different cell surface receptors.[8]

In addition, the proliferation and survival of tumor cells also depend on the interactions between cells and their environment, including the extracellular matrix (ECM).[9,10] Recent findings also gave assertion of the functional crosstalk between certain cell adhesion molecules and receptor tyrosine kinases, suggesting that they may contribute to developing chemo- and radioresistance.[11,12] The coactivation of interacting multiple receptor tyrosine kinases and cell adhesion molecules may drive redundant inputs into the cytoplasm, maintain downstream signaling, and affect the response of tumor cells to targeted therapies.[13–16] Integrins (eg, the α5β1 heterodimer) form multimeric clusters of diverse proteins in focal adhesion complexes that drive signaling to prevent apoptosis.[17,18] ErbB1 is also localized at these sites and can give rise to activation of the focal adhesion kinase (FAK) and the PI3K–Akt/PKB pathway, which promotes cell survival through inactivation of Bad and caspase-9, as well as the transcription factor FKHRL-I.[19,20] Interaction between ErbB1 and integrin-β1 also enhances tumor cell detachment, migration, and metastic ability[21] by displacing tensin-3 from the cytoplasmic tail of integrin-β1, resulting in the disassembly of the actin cytoskeleton machinery.[22]

The integrin-β1 mediated PI3K/Akt-PKB signaling was also shown to be critically involved in glioma cell adhesion and prolonged cell survival.[23] Moreover, most recent findings highlighted integrin-β1 inhibitors as potentially promising radiosensitizers for glioblastoma in vitro.[24] Accordingly, interactions of ErbB1 and integrin-β1 could play an important role in the development of increased radioresistance and present a novel therapeutic target. The importance of these interactions has thus far been raised on the basis of in vitro and xenograft models. However, expression profiles and molecular associations of ErbB and integrin molecules may differ on individual human glioblastoma tumors in situ, which may prejudice treatment and patient outcome. Steadily improving fluorescence resonance energy transfer (FRET) techniques have now evolved to the potential of characterizing molecular interactions in tissue sections.[25,26] Indeed, FRET results precisely quantitating molecular interactions on individual clinical tumor samples in situ could be conjoined with clinical data to better define prognosis or optimal therapy.[27,28]

In this article, we show a method for quantitatively assessing in situ molecular interactions of ErbB1 and integrin-β1 by confocal microscopic FRET measurements on intraoperative fresh frozen tissue sections of grade II and IV astrocytomas. Furthermore, 2 cellular model systems showing expression profiles similar to low- and high-grade astrocytomas have been generated to show that increased ErbB1 expression causes the presence of excess integrin-β1 in the membrane. Consequential shift of signaling from ErbB1 homoassociation to ErbB1–integrin-β1 heteroassociation and toward the activation of the PI3K-Akt/PKB pathway may result in increased radioresistance that can be overcome by inhibition of PI3K. This enhanced interaction is also detectable in grade IV vs grade II astrocytoma and appears to be an efficient predictor of patient survival and disease recurrence.

Materials and Methods

Fresh Frozen Sections

Tumor samples collected during neurosurgical procedures of patients with glioma were stored at −80°C in the Brain Tumor and Tissue Bank of the Department of Neurosurgery with the permission of the National Research Ethical Committee. Each patient signed an informed consent form before surgery. Histological classification was done during routine pathological examination. Samples were snap-frozen in isopentane (Sigma-Aldrich, St. Louis, MO) cooled in liquid N_2. After embedding in Tissue-Tek O.C.T. (Sakura Finetek, Torrance, CA), 15-μm thick sections were cut with a Shandon Cryotome (AS-0620E, ThermoFisher Scientific Inc., Waltham, MA) at −20°C. Sections on silane-coated slides were dried, fixed in 4% PFA-PBS for 30 min, blocked in 1% BSA-PBS for 30 min, and labeled with 20 μg/mL Cy3 conjugated anti-ErbB1 antibody (Mab528) and 20 μg/mL Cy5 conjugated anti-integrin-β1 antibody (clone TS2) overnight in a wet chamber at 4°C, washed 3 times, and mounted in glycerol.

Cell Cultures

The parental U251 NCI cell line (National Cancer Institute, Bethesda, MD; hereafter, U251) and subclones were stored frozen in LN_2, regularly verified as negative for mycoplasma, and used within 6 months. Cells were grown to subconfluence in MEM EBSS, 10% FCS, and nonessential amino acids at 37°C, in 5% CO_2. We have used subclones c5, c9, and c55 with increasing amounts of chromosome 7, paralleled with increasing radioresistance.[29] For control, we used the U251 Hyg+ subclone resistant to hygromycin B used for selection at 0.4 mg/mL.

Stable Transfection of ErbB1

The erbB1 gene in pCDNA3 (kind gift from Yosef Yarden, Weizmann Institute of Science, Rehovot, IL) was electroporated into U251 (Amaxa, Cologne, Germany) with solution V and protocol T-20. Cells were selected with 0.4 mg/mL geneticin, and sorted in a FACSVantage SE with DiVa option (Becton Dickinson, Franklin Lakes, NJ) into subclones of low, medium, and high ErbB1 expressors. A low ErbB1 (~150 000 copies per cell, U251_E1L) and a high ErbB1 (~1 million copies per cell, U251_E1H) transfectant subline was created and stocked and used as a stable expression system under selection pressure for 3–4 passages. Cells were only passaged beyond this (up to passage 28) for testing stability of expression.

Determination of Radiosensitivity

Radiosensitivity was determined from colony forming after exposure to 0, 2, 4, 6, and 8 Gy of ^{60}Co γ irradiation. Aliquots at 2 Gy were also treated with 20 nM wortmannin (Sigma-Aldrich, St. Louis, MO) starting 1 h before irradiation. Six replicates of 200 single cells of each subline were placed and incubated until attachment in a flat-bottom 96-well plate and cultured in and irradiated through indicator-free DMEM medium. To minimize radiation scattering, plates were submerged into water bath and irradiating doses were corrected for the absorbance of the thickness of liquid layer. Seven days after irradiation, methylene blue– (0.2% w/v in 70% ethanol) stained colonies were counted. Colonies were imaged in an imaging cytometer (CompuCyte Corp, Cambridge, MA) using 633 nm transmission images for colony counting and contouring of clusters.

Surviving fractions were calculated and normalized according to

$$SF(D) = \frac{\text{Colonies Counted}}{\text{Number of Cells Plated} \cdot PE_{D_0}}, \quad (1)$$

where PE_{D_0} is the plating efficiency of cells receiving no radiation:

$$PE_{D_0} = \left[\frac{\text{Colonies Counted}}{\text{Number of Cells Plated}}\right]_{\text{Dose}=0}. \quad (2)$$

Survival curves were fitted and plotted using the Linear Quadratic Model in Sigmaplot v10.0 (Systat Software, Inc., Chicago, IL) according to

$$S(D) = e^{-(\alpha \cdot D + \beta \cdot D^2)}, \quad (3)$$

where D denotes the irradiation dose, α (Gy^{-1}) is the initial slope of the survival curve attributed to DNA double strand breaks, and β (Gy^{-2}) characterizes single strand breaks.

Western Blot Analysis

Cells were serum starved overnight, then treated with 50 ng/mL EGF for 30 min at 37°C. PBS-washed pellets were solubilized in 5× SDS-sample buffer, sonicated, and centrifuged (16 000 × g, 5 min), and supernatants were subjected to standard SDS-PAGE (7% gel), followed by ECL-visualized, peroxidase-based immunoblotting. Akt and pAkt were detected using specific antibodies (Upstate/Millipore, Billerica, MA); β-actin (AC40, Sigma-Aldrich, St. Louis, MO) was the loading control. Signal intensity of Akt or pAkt was quantified, corrected for background values, and normalized to β-actin.

Antibodies

Monoclonal antibodies against ErbB1, integrin-β1, β2-microglobulin, and HLA-A, B, and C were purified from supernatants of the hybridoma cell lines 528 (IgG_{2a}, #HB-8509), TS2/16.2.1 (IgG1, #HB-243), L368 ($IgG1_{\kappa}$, #HB-149), and W6/32 (IgG_{2a}, #HB-95), respectively (ATCC, Manassas, VA) with use of Sepharose 4B Fast Flow Protein G beads in the case of IgG_{2a} and protein A beads in the case of IgG_1 (Sigma-Aldrich, St. Louis, MO). Labeling of antibodies with Cy3, Cy5 (Amersham Biosciences Europe, Freiburg, Germany), AlexaFluor 546, AlexaFluor 647, and X-FITC (Molecular Probes, Invitrogen Corp., CA) was done in accordance with the manufacturers' specifications. The dye to protein labeling ratio determined by spectrophotometry was in the range of 2:1–3:1.

Labeling of Cells with Antibodies

For flow cytometric measurements, cells were trypsinized, resuspended at 1×10^6 cells in 50 μL PBS with 0.1% bovine serum albumin (BSA), and labeled with saturating concentration (10–20 μg/mL) of AlexaFluor 546 and/or AlexaFluor 647–conjugated antibodies on ice (4°C) for 30 min. Cells were then washed 3× in PBS and fixed in 500 μL 1% formaldehyde-PBS.

For microscopic measurements, adherent cells on Lab-Tek II chambered coverglass (Nalge Nunc International, Rochester, NY) were washed 3× in PBS, labeled with saturating concentrations of X-FITC, Cy3- or Cy5-conjugated antibodies (singly or in combination) on ice for 30 min, and washed 3× in PBS and fixed in 500 μL of 4% formaldehyde-PBS for 20 min.

Flow Cytometric Determination of Cell Surface Receptor Expression

Receptor expression was quantitated on a FACSVantage SE with DiVa option (Becton Dickinson, Franklin Lakes, NJ) using the FL6 channel (excitation: 633 nm, detection: 650 nm LP) in linear mode. The background corrected mean of histograms from 20 000 events was converted to antigen numbers using QIFIKIT (DakoCytomation, Glostrup, Denmark) according to the manufacturer's instructions. Label-free 528 or TS2 primary antibodies were detected using AlexaFluor 647–conjugated goat-

anti-mouse (H + L) secondary antibodies (Molecular Probes, Invitrogen Corp., CA).

Flow Cytometric Fluorescence Resonance Energy Transfer Measurements (FCET)

To determine the homo- and heteroassociation states of the labeled receptors, flow cytometric FRET measurements with cell-by-cell correction for autofluorescence[30] were performed on a FACSVantage SE with DiVa option (Becton Dickinson). Cellular autofluorescence was measured in the FL1 channel (excitation: 488 nm, detection: 530/30 nm BP). Donor intensities were recorded in the FL4 channel (585/42 nm BP); acceptor and sensitized acceptor intensities were detected (650 nm LP) in channels FL6 and FL5, respectively. Donor and acceptor excitation was with 532 nm and 633 nm laser lines. Calculation of cell-by-cell FRET efficiency was done in REFLEX.[31] FRET efficiencies are presented as mean values of approximately normally distributed, unimodal FRET histograms of 20 000 cells, indicating standard error of the mean (SEM) as error bars.

Confocal Microscopy

A Zeiss LSM 510 CLSM (Carl Zeiss, Jena, Germany) with a Plan-Apochromat 63×/1.40NA oil immersion objective and an UV/488/543/633 beam splitter was used. X-FITC, Cy3, and Cy5 fluorophores were excited at 488, 543, and 633 nm and detected through 505–535, 560–605 nm bandpass, and 650 nm longpass filters, respectively; 1–3 μm thick, 4-times averaged optical sections (512 × 512 pixels at 12 bit) were imaged in multitrack mode to avoid crosstalk between channels. For assessing expression levels on tissue sections, images were taken in tile mode.

Donor Photobleaching FRET Method (dbFRET)

In dbFRET,[32] the E FRET efficiency is

$$E = 1 - \frac{\tau_{ble}}{\tau^{A}_{ble}}, \qquad (4)$$

where, τ_{ble} and τ^{A}_{ble} are the photobleaching time constants in the absence and presence of the acceptor. Specimens were bleached with 50 scans at 488 nm with high laser power. Images were fitted using the dbFRET software,[33] yielding images of the photobleaching time constants.

Acceptor Photobleaching Method (abFRET)

FRET efficiency (*E)* in each pixel was measured using the acceptor photobleaching protocol and calculated as follows[34]:

$$E = 1 - \frac{F^{B}_{D(i,j)} - S^{avr}_{4} \cdot F^{B}_{A(i,j)}}{\gamma^{avr} \cdot F^{A}_{D(i,j)}}, \qquad (5)$$

where $F^{B}_{D(i,j)}$ and $F^{A}_{D(i,j)}$ are the background subtracted donor fluorescence values before and after photobleaching the acceptor, respectively, and $F^{B}_{A(i,j)}$ denotes the background subtracted acceptor fluorescence value before photobleaching the acceptor in pixels (i,j). $\gamma^{avr}$and S^{avr}_{4} are factors correcting for the photobleaching of the donor and crosstalk of the acceptor into the donor channel.[35] Measurement was done on the LSM 510 described above and evaluated using the ImageJ plugin AccPbFRET.[35]

Two-Sided FRET Experiments on U251 Transfectant Subclones (tsFRET)

Pixel-by-pixel relationship of ErbB1 homoassociation and ErbB1–integrin-β1 heteroassociation was analyzed using two-sided FRET.[36] After labeling ErbB1 with a mixture of X-FITC and Cy3-conjugated 528 Abs, and integrin-β1 with Cy5-TS2, abFRET quantifying ErbB1-integrin heteroassociation was done for the Cy5-Cy3 FRET pair, followed by dbFRET on X-FITC with or without the Cy3 acceptor to characterize ErbB1 homoassociation in the same pixels. Correlated values are displayed on contour plots (Sigmaplot, Systat Software, Inc., Chicago, IL; Igor Pro, WaveMetrics, Inc., Portland, OR).

Statistical Analysis

Analysis was done using SigmaStat 3.5.0.54 (Systat Software, Inc.). Parameters of grade II and IV astrocytic tumor groups were compared using Student's *t* test or in the absence of normality with Mann-Whitney rank sum tests after checking normality according to Kolmogorov-Smirnov with Lilliefors' correction. Normally distributed variables of >2 classes were compared using ANOVA, followed by Tukey's post hoc test. Predicting power of ErbB1 and integrin-β1 expression and ErbB1–integrin-β1 heteroassociation on recurrence time was assessed by stepwise forward multiple regression and on the grade of tumor by stepwise multiple binary logistic regression. Overall and relapse-free survival were analyzed using the Kaplan-Meier method comparing grade II against grade IV tumors, as well as pairs of groups created by splitting the whole cohort into below and above average values of ErbB1 or integrin-β1 expression or ErbB1–integrin-β1 heteroassociation. Patients enrolled later than the start of the observation time and still alive at the end of the study were censored from further analysis at their survival time point. Patients who underwent incomplete tumor resection were also censored in the analysis of relapse-free survival. Statistical comparison and the estimation of *P* were done using the log-rank test.

Results

ErbB1 and Integrin-β1 Expression Increases with Elevated Radioresistance and Amount of Extra Chromosome 7 Material in U251 Subclones

Previously, the radioresistance of U251 subclones Hyg+, c5, c9, and c55, bearing increasing copy numbers of extra choromosome 7 fragments, was determined by agar colony forming assay as LD_{50} of 4.0, 4.7, 5.0, and 5.7 Gy, respectively.[29] Because previous results indicated the involvement

of integrins in chemo and radiosensitivity,[37] we have done a protein level screen of integrins αV, α1, α2, α4, α6, β1, β3, β4, and β5 on these subclones (Supplementary Fig. S1). This revealed that, in parallel with increasing extra chromosome 7 material and radioresistance, Hyg+, c5, c9, and c55 subclones expressed not only increasing numbers of ErbB1 (65, 77, 83, and 270 thousand per cell) but also increasing numbers of integrin-β1 (360, 400, 420, and 540 thousand per cell), respectively (Fig. 1A).

Ectopic Overexpression of ErbB1 Alone in U251 Also Induces Higher Integrin-β1 Levels

Because chr. 7 does not carry the integrin-β1 gene, the coexpression patterns of ErbB1 and integrin-β1 were also tested in U251 stably transfected with erbB1. The high and low ErbB1 expressing U251_E1H and E1L were followed through 28 passages by flow cytometry. The U251_E1H subline incrementally split into 2 subpopulations: a low and a high ErbB1 expresser, denoted U251_E1H/L and U251_E1H/H, respectively. Initially, all sublines expressed an increased number of ErbB1, accompanied by an increased expression of integrin-β1, compared with the parental U251 cell line (Fig. 1B). The ErbB1 and integrin-β1 expression of the transfectants E1L, E1H/L, and E1H/H was stably sustained (Fig. 1C), whereas the ratio of the E1H/H subpopulation in the U251_E1H subline decreased gradually over the passages (Fig. 1D). Of interest, the U251_E1H/H subpopulation did not show statistically significant further increase of integrin-β1 expression over the E1L, despite the extreme increase in ErbB1.

Excess ErbB1 and Integrin-β1 Contribute to Postirradiation Survival, Whereas Additional Surplus ErbB1 Contributes Primarily to Colony Forming Ability

After irradiation, the surviving fraction of U251_E1L and freshly sorted E1H transfectants increased parallel with their increasing ErbB1 and integrin-β1 expression levels, but additional increase in the ErbB1 expression on the U251_E1H subline did not contribute to a significantly higher survival rate (Fig. 2A). In the linear-quadratic model, both the parameters α and β significantly differed between the parent U251 and its transfectants, but not between the 2 transfectants E1H and E1L (Fig. 2A), hinting at the dependence of these factors on the amount of integrin-β1 present in the membrane. However, the presence of additional surplus ErbB1 receptors promoted the colony forming capability of the high ErbB1-expressing U251_E1H, compared with the low ErbB1 parental U251 and even with the intermediate ErbB1 U251_E1L (Fig. 2B).

Additional Integrin-β1 Is Crucial for Increasing Akt-Dependent Radiation Resistance, which Can Be Overcome by the Inhibition of PI3K

To gain insight into the signaling mechanisms behind growing radioresistance, we assessed the involvement of the PI3K/Akt survival pathway, a suspected outcome of ErbB1–integrin-β1 crosstalk. Western blot of Akt and pAkt proteins disclosed a significant 85% increase in the pAkt levels of both U251_E1L and E1H transfectant sublines, as quantitated by densitometry (Fig. 2C). In addition, the pAkt/Akt ratio on EGF treatment in both U251_E1L and E1H increased (1.6 ± 0.2 and 1.8 ± 0.2, respectively), compared with the parental U251 cell line (1.1 ± 0.1). The additional increase of pAkt/Akt ratio in E1H, opposed to E1L transfectants, was low, compared with the increase in ErbB1 expression (Fig. 2D). Increased radioresistance of U251_E1L over U251 could be reverted by inhibiting PI3K with wortmannin (Fig. 2E).

ErbB1 Homoassociation Decreases, but ErbB1–Integrin-β1 Heteroassociation Increases with Increasing ErbB1 and Integrin-β1 Expression Levels in U251 Subclones

To assess the possible physical interaction between ErbB1 and integrin-β1 behind increased Akt activation, we measured FRET efficiency between ErbB1 molecules and between ErbB1 and integrin-β1 first by flow cytometry. MHC-I–β2-microglobulin intramolecular FRET efficiency was determined for positive reference control ($28\% \pm 2\%$). The results revealed anticorrelation between the decreasing ErbB1 homoassociation states and the increasing ErbB1–integrin-β1 heteroassociation rates for Hyg+, c5, c9, and c55 U251 subclones, respectively (Fig. 3A). Flow cytometric FRET experiments also disclosed anti-correlation between decreasing ErbB1 homoassociation and increasing ErbB1–integrin-β1 heteroassociation in the following order: U251 parental cell line, U251_E1L, E1H/L, and E1H/H transfectants (Fig. 3A). As a control, FRET was also measured in the integrin-β1–ErbB1 direction by reversing the donor-acceptor labeling, and similar tendency was observed as previously (2%, 3%, 4%, and 18%), which indicates that the observed reciprocity of interactions is independent of stochiometry and cannot be considered a simple random mass effect. In line with the similar expression profiles of the U251_E1L and E1H/L sublines, their FRET values for ErbB1 homoassociation and ErbB1–integrin-β1 heteroassociation were nearly identical (Fig. 3B).

Integrin-β1 Recruits ErbB1 from ErbB1 Homoclusters to Shift the Balance toward ErbB1–integrin-β1 Heteroassociation

To explore the complementary nature of ErbB1-integrin interactions at the submicron scale of membrane domains, two-sided microscopic FRET experiments, demonstrated schematically on Fig. 3C, were done on U251_E1H/L and E1H/H. These enabled the correlated measurement of ErbB1 homoassociation and ErbB1–integrin-β1 heteroassociation (Fig. 3D); the contour plots match these 2 quantities pixel by pixel. Both E1H/L and E1H/H show anticorrelation between the ErbB1 homoassociation and ErbB1–integrin-β1 heteroassociation, which can be interpreted as a sign of overexpressed integrins acquiring molecular proximity to ErbB1 at the price of disrupting some ErbB1 homoassociation. Overall tendencies of stronger hetero- and lesser homoassociation in E1H/H are coherent with the flow cytometric data.

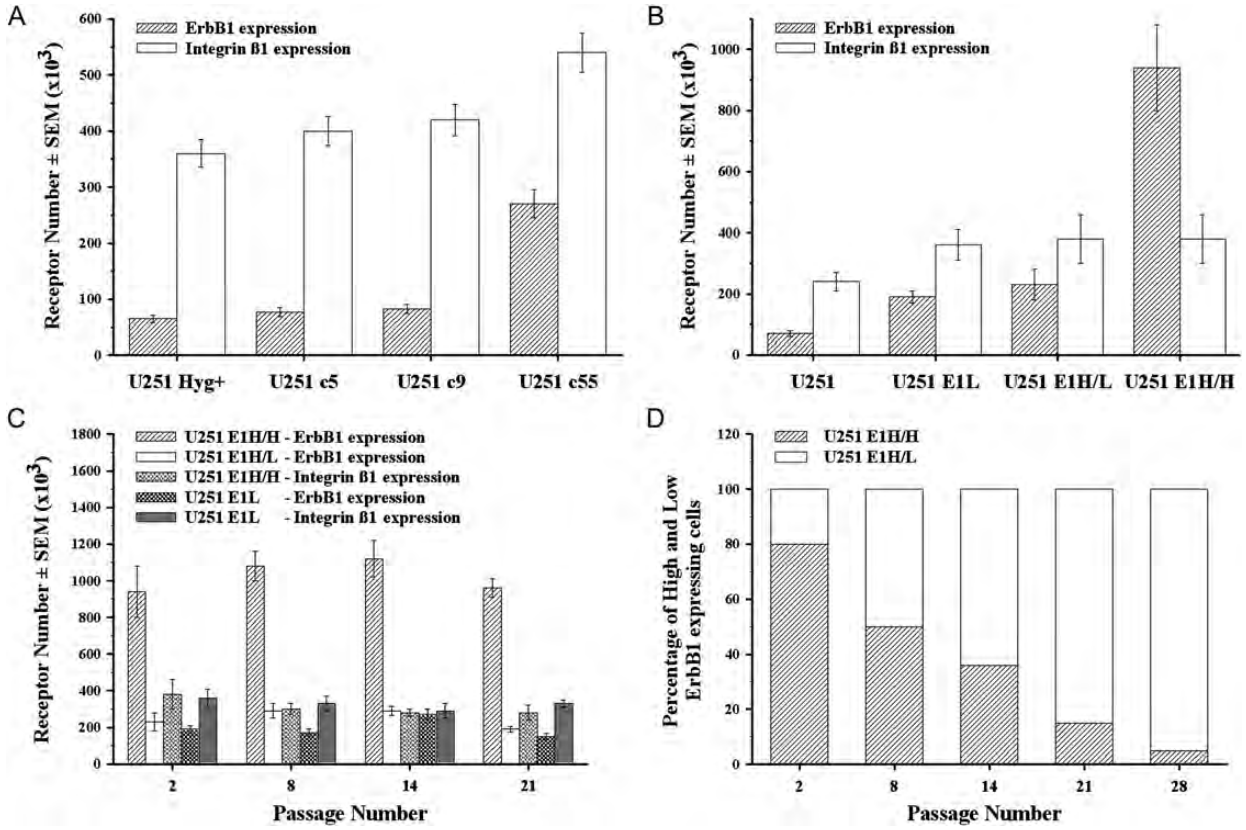

Fig. 1. Expression profile and through-passage stability of U251 sublines armed with extra chromosome 7 (c5, c9, c55) or transfected with erbB1 gene (E1L, E1H/L, E1H/H). U251 subclones were labeled for ErbB1 with AlexaFluor 546-528 and for integrin-β1 with AlexaFluor 647-TS2 antibodies, as described in the Material and Methods. (A and B) Number of ErbB1 (▨) and integrin-β1 (□) molecules on the cell surface of U251 subclones transferred with extra chromosome 7 material (A) or transfected with erbB1 gene (B) were quantitated by flow cytometry using QIFIKIT. (C) Number of ErbB1 on U251_E1H/H (▨), E1H/L (□), and E1L (▪) and number of integrin-β1 on U251_E1H/H (⊠) and E1L (■) subclones over 28 passages. (D) Percentage of high (E1H/H) and low (E1H/L) ErbB1 expressing subpopulations of U251_E1H transfectant subline gradually splitting into 2 over the passages.

Grade IV Astrocytoma Samples Exhibit Higher ErbB1 and Higher Integrin-β1 Expression than do Grade II Astrocytoma Samples

To correlate the in vitro findings with the clinic, we determined the ErbB1 and integrin-β1 expression on fresh frozen tissue sections of grade II and grade IV astrocytoma tumors removed during surgery. Ten patients with grade II (age, 18–59 years; mean age, 37.8 years, 5 males and 5 females) and 10 with grade IV (age, 42–73 years; mean age, 61.4 years; 3 males and 7 females) astrocytoma had samples obtained. Relevant clinical data are summarized in Table 1. Background corrected mean fluorescence intensities of immunofluorescence-labeled tissue sections were overall higher in grade IV than in grade II tumors both for ErbB1 and for integrin-β1 (Fig. 4A).

ErbB1–Integrin-β1 Molecular Interaction Is Increased in Grade IV Astrocytoma, Compared with Grade II

We have also analyzed the molecular interaction of ErbB1 and integrin-β1 on fresh frozen tissue sections in situ, using the confocal microscopic abFRET technique. As a positive control, MHC-I–β2-microglobulin intramolecular FRET efficiency was determined and was 14% ± 0.3%. Images of ErbB1 (FRET donor fluorescence), integrin-β1 (FRET acceptor fluorescence), and FRET on grade II and grade IV astrocytoma samples (TC515 and T82, respectively) are shown in Fig. 4B. The indexed color FRET images demonstrate well that the higher grade astrocytoma (T82) showed higher ErbB1–integrin-β1 heteroassociation than did the lower grade sample (TC515). Overall, abFRET on grade IV tumors showed stronger ErbB1–integrin-β1 heteroassociation, compared with grade II tumors (Fig. 4C). The clear separation of the 2 disease groups was verified by binary logistic regression.

Heteroassociation of ErbB1 and Integrin-β1 Alone Is a Potential Predictor of Therapy Outcome in Astrocytomas

Grade IV tumors showed significantly higher integrin-β1 expression levels than did grade II tumors ($P = .038$); however, despite higher mean values and remarkable salience of ErbB1 expression levels in 2 cases of grade IV samples, the difference of ErbB1 levels between grade II

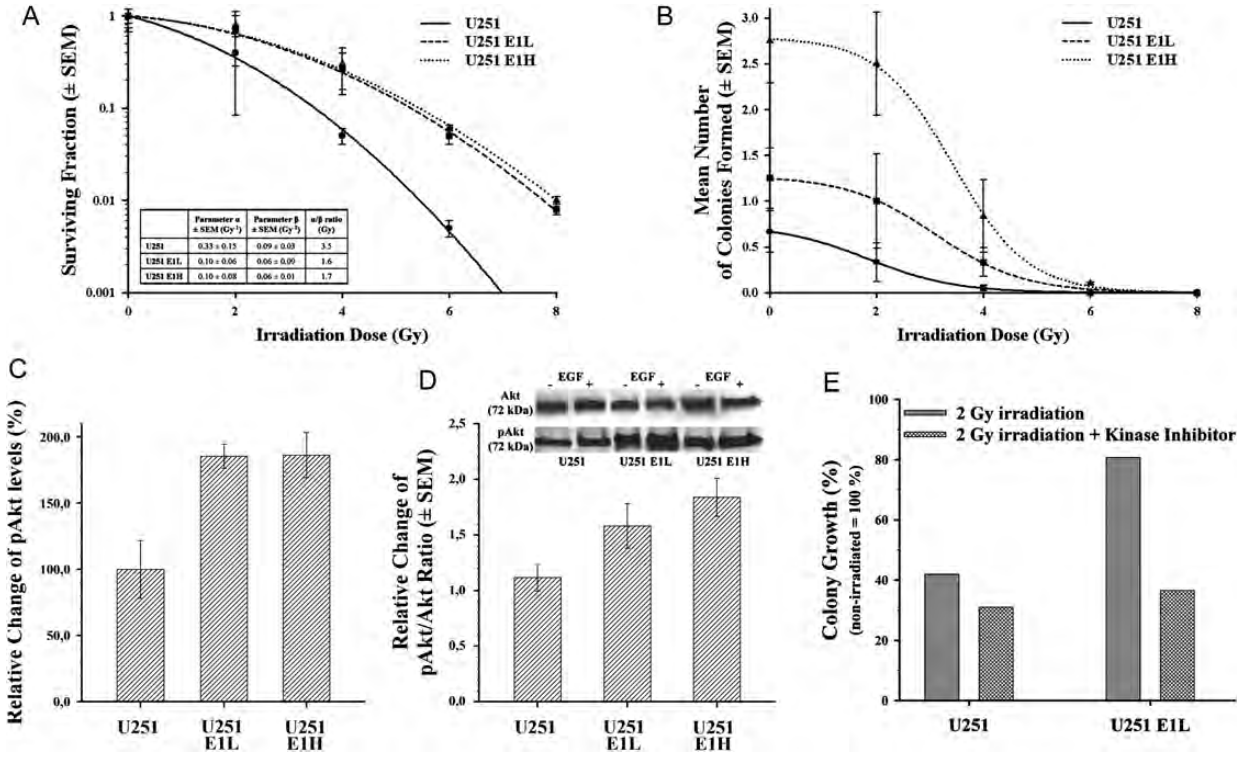

Fig. 2. Survival rate, colony forming capability after ionizing radiation and PI3K inhibition, and change in the pAkt/Akt equilibrium after EGF treatment. (A) Surviving fraction of U251 parental (●—●), U251_E1L (■– – –■), and U251_E1H (▲. . .▲) subclones after exposure to 2, 4, 6, and 8 Gy irradiating dose. On every irradiated U251 cell line, the parameter α, describing the direct ionizing effect; the parameter β, reflecting the sublethal effect of the irradiation; and the α/β ratio, giving the irradiating dose, at which the linear and quadratic components of cell killing are equal, were calculated according to the linear quadratic model. (B) Colony forming ability of U251 parental (●—●), U251_E1L (■– – –■), and U251_E1H (▲. . .▲) sublines after exposure to 2, 4, 6, and 8 Gy irradiating dose. (C) The relative change of pAkt levels in U251 and its transfectant sublines determined by densitometry of Western blots (mean ± SD of 3 experiments). (D) The pAkt/Akt ratio after EGF treatment and corresponding Western blot image of starved U251 transfectant sublines. Of note, survival rate and increase of pAkt in U251_E1H and U251_E1L transfectants did not show significant difference, whereas their colony forming ability was remarkably higher in U251_E1H and was also accompanied by a higher responsivity of Akt phosphorylation to EGF stimulus. (E) Relative percentage of well coverage in comparison to the respective, nonirradiated U251 and U251_E1L subclones after exposure to 2 Gy irradiation alone (▩) or combined with the inhibition of PI3K with wortmannin (▩).

and IV tumors was not significant ($P = .379$). Coherent with the great difference in ErbB1–integrin-β1 heteroassociation states between the two tumor classes ($P < .001$), stepwise binary logistic regression identified this parameter as a single determinant of tumor grade out of ErbB1 expression, integrin-β1 expression, and the FRET efficiency between these 2 molecules (odds ratio =8716) (Fig. 4D). In addition, multiple stepwise linear regression highlighted FRET efficiency as the predictor of time to relapse for both pooled grade II and IV samples and for the grade IV cases alone ($P = .094$ and .085, respectively). Analyzing survival times of pooled grade II and grade IV cases by multiple stepwise linear regression showed that, in addition to ErbB1–integrin-β1 interaction ($P < .001$), the expression level of integrin-β1 significantly ($P = .05$) contributes to the prediction of survival.

Overall, survival among patients was coherent with known differences between grade II and grade IV glioblastoma (Fig. 5). All patients with grade II tumors survived for over a year after surgery. In this group, 5 patients received radiotherapy based on the severity of size, localization, and postoperative recurrence. All of them developed relapse, one of which (T80′) transformed into malignant glioblastoma. Survival was 16–77 months. Of the nonirradiated grade II astrocytomas, 3 also recurred: T33 and TC416 after 48 and 33 months, with survival >6 years and 40 months, respectively, whereas for T86/B, relapse and survival were 14 and 16 months, respectively, after surgery. Notably, tumor T86/B, with the shortest survival, and T80′, which gave rise to a grade IV recurrence, showed the highest ErbB1–integrin-β1 heteroassociation in the grade II group (Fig. 4C).

All patients with grade IV tumors received radiotherapy, and all of them developed recurrence: 7 patients within 6 months and 2 (T71, T74) after 12–13 months. In the case of T10/B, only a biopsy could be managed. The 2 patients developing the earliest recurrence (2 months, T53 and T82) and showing the shortest survival (4 months) bore tumors with the highest ErbB1 and integrin-β1 expression levels and the greatest extent of ErbB1–integrin-β1 heteroassociation. Furthermore, the

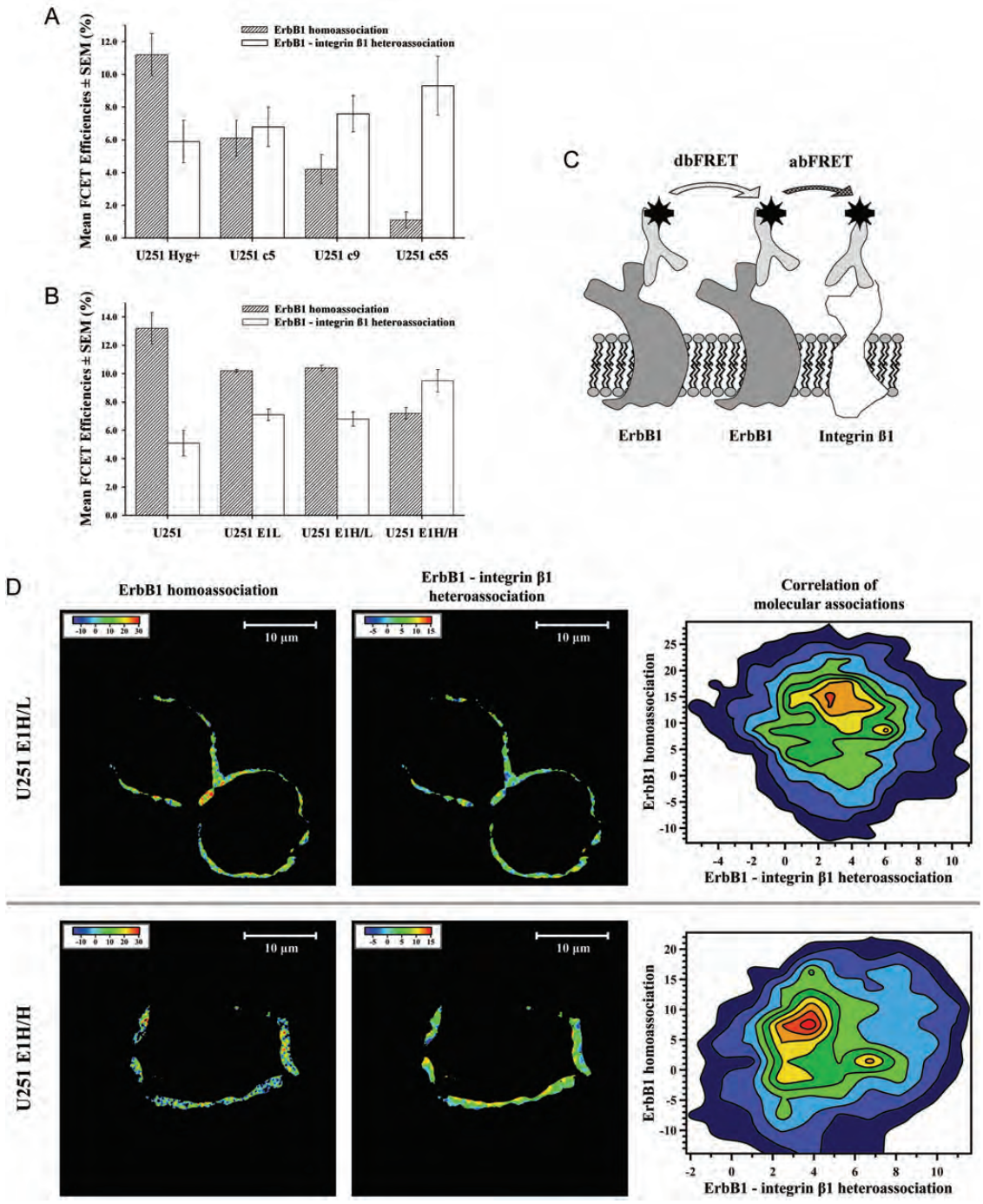

Fig. 3. ErbB1 homoassociation, ErbB1–integrin-β1 heteroassociation states, and correlation of the molecular associations in tsFRET experiments on U251 subclones. On U251 subclones, double-labeled for ErbB1 with AlexaFluor 546–528 and for integrin-β1 with AlexaFluor 647-TS2 antibodies, FCET experiments were performed as described previously. (A and B) Autofluorescence-corrected FCET efficiency values of ErbB1 homoassociation (▨) and ErbB1–integrin-β1 heteroassociation (□) were calculated from flow cytometric data with a custom written software Reflex on U251 subclones transferred with chromosome 7 material (A) or transfected with erbB1 gene (B). MHC-I – β_2-microglobulin intra-molecular FCET efficiency was determined as positive reference control (27.6% ± 1.9%). (C) Schematic model of tsFRET experiments. U251 transfectant cells were triple-labeled for ErbB1 with XFITC-528 (*left*) and Cy3-528 (*middle*) and for integrin-β1 with Cy5-TS2 (*right*) antibodies. Consecutive abFRET (between Cy3-528 and Cy5-TS2) and dbFRET (between XFITC-528 and Cy3-528) measurements were performed. (D) The false color maps of dbFRET (ErbB1 homoassociation) and abFRET (ErbB1–integrin-β1 heteroassociation) efficiencies and the contour plots of the corresponding pixel-by-pixel dbFRET and abFRET efficiency values of U251_E1H/L and E1H/H subpopulations are shown. Note the increase in ErbB1–integrin-β1 heteroassociation and the decrease in ErbB1 homoassociation on the U251_E1H/H subpopulation. Also consider that 2 discrete peaks are distinguishable on both corresponding contour plots.

Table 1. Clinical findings, therapy, and survival profiles in study patients

No.	Code	Therapy	Relaps	Survival
Astrocytoma, Gr. II.				
II./1.	T33	Op+Op	48 months	>82 months (alive)
II./2.	T34	Op+Rx	50 months	77 months
II./3.	T59	Op+Rx	residual tumor	42 months
II./4.	T80′	Op+Rx+Op+Op	15 months	31 months
II./5.	T86/B	Op+T	14 months	16 months
II./6.	TC515	Op	-	>34 months (alive)
II./7.	TC416	Op	33 months	>40 months (alive)
II./8.	TC497	Op+Op+Rx	32 months	>36 months (alive)
II./9.	TC326[a]	Op+Op	-	>41 months (alive)
II./10.	TC493	Op+Rx	3 months	16 months
Astrocytoma, Gr. IV. Glioblastoma multiforme				
IV./1.	T10/B	Op+Rx	biopsy	10 months
IV./2.	T32	Op+Rx	4 months	7 months
IV./3.	T53	Op+Rx+Op+T	2 months	4 months
IV./4.	T65	Op+Rx+Op	4 months	8 months
IV./5.	T67	Op+Rx	4 months	7 months
IV./6.	T71	Op+Rx+Op+Rx+Op	12, 12, 6 months	40 months
IV./7.	T74	Op+Rx	13 months	16 months
IV./8.	T75*	Op+Rx	4 months	10 months
IV./9.	T76*	Op+Rx+BCNU	4 months	8 months
IV./10.	T82	Op+Rx	2 months	4 months

List of the intraoperative astrocytoma samples and the clinical findings, therapeutic interventions, outcomes, and survival profiles of the corresponding patients with glial tumors are summarized.
Abbreviations: BCNU, 1,3-bis(2-chloroethyl)-1-nitrosourea (carmustine) chemotherapy; Op, operation; Rx, radiotherapy; T, temozolomide chemotherapy.
[a]In the case of TC326, the start of the follow-up time in this study was actually a second operation; the tumor first had been diagnosed and resected as a grade I astrocytoma 7 years previously.

lowest ErbB1–integrin-β1 heteroassociation was seen on T71, which developed multiple recurrences, was resected 3 times, irradiated after every surgical intervention, and survived 40 months, as opposed to the <6-month postrelapse and 4–16 months overall survival in the rest of this cohort.

Kaplan-Meier analysis was used to compare overall and progression-free survival of grade II and grade IV groups and groups formed by splitting the pooled samples into below and above the overall mean expression level of ErbB1, integrin-β1, and mean heteroassociation state. Survival was determined best and equally well by histopathological grading and ErbB1-integrin heteroassociation ($P < .001$), whereas ErbB1 and integrin-β1 levels showed less, but still significant differences ($P = .014$, $P = .004$) (Fig. 5). A similar trend was apparent for progression-free survival, with $P < .001$ for grade, integrin-β1 expression and heteroassociation and with $P = .014$ for ErbB1 expression. (Supplementary Fig. S2).

Discussion

Over the past decades, intensive research has been focused on combining therapeutic modalities in the treatment of invasive astrocytomas. However, despite ever-broadening therapeutic options, prognosis in patients with high-grade astrocytic tumors still remains highly unfavorable. Perifocal recurrences emerge from unresectable scattered tumor cells migrated to the surrounding brain tissue. Molecular data indicate that integrins (eg, the αVβ1 heterodimer) contribute to this infiltrative migration of brain tumor cells, and their expression correlates with tumor type and grade.[38] Indeed, the term "cell adhesion mediated therapy resistance" of glioblastoma cells is now also steadily evolving to describe the potential role of survival pathways originating from cell-cell or cell-ECM interactions.[39] Synergism of radiotherapy with inhibiting downstream signaling of ErbB1 and integrin proteins has been proposed.[40–42] ErbB1 has recently become the target of small-molecule tyrosine-kinase inhibitors in patients with glioblastoma,[43–45] and inhibition of integrin αVβ3 signaling with the RGD mimetic peptide cilengitide has reached the clinical phase;[46] however, the positive effects were more likely attributable to direct effects on endothelial cells and tumor vascularization.[47] This assumption correlates well with the very low expression of integrin β3 on the U251 glioma cells that were used (Supplementary Fig. S1).

These emerging findings call for establishing further, cell function–related diagnostic methods that warrant the application of certain single or combined therapeutic

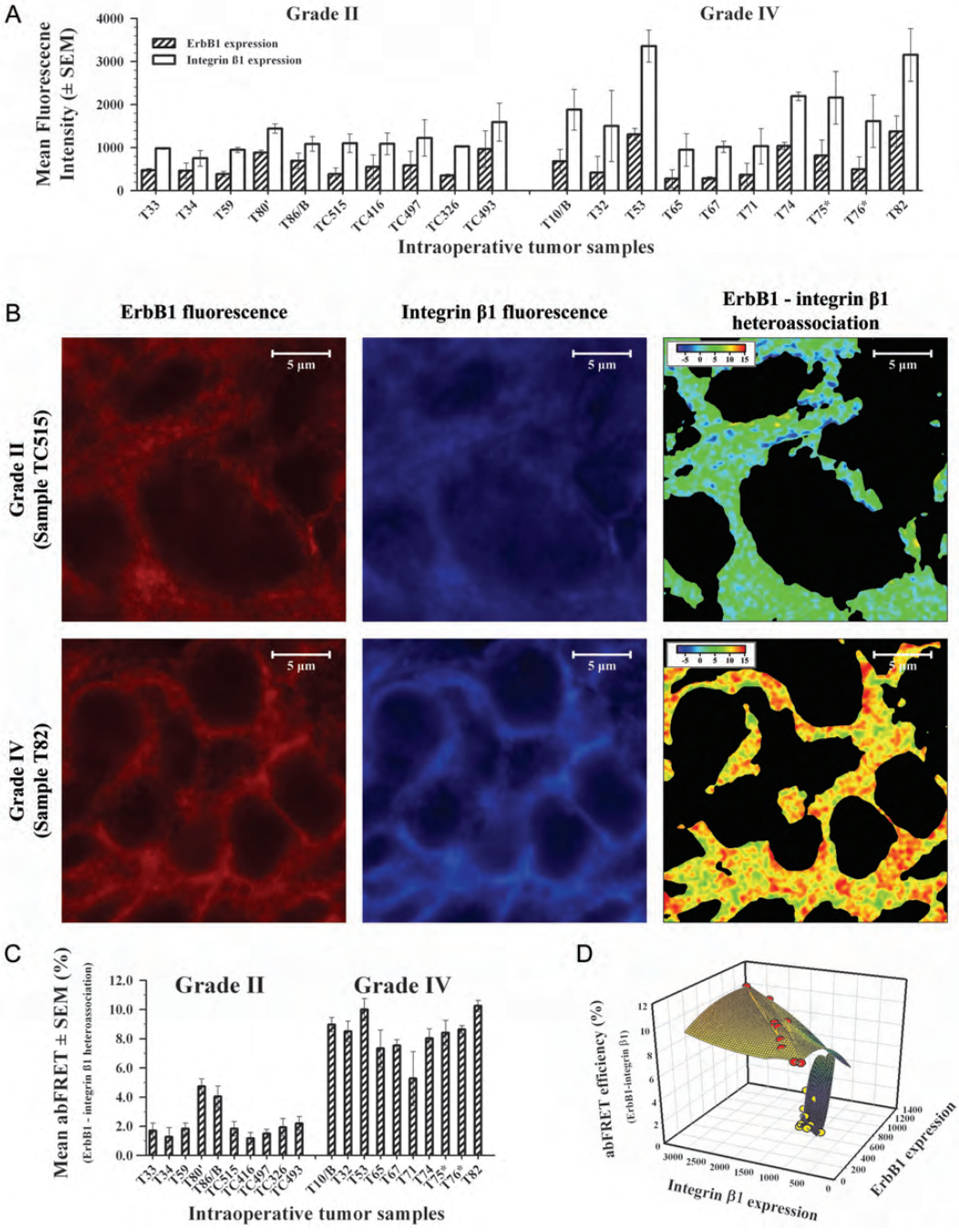

Fig. 4. Expression profiles and ErbB1–integrin-β1 heteroassociation states on clinical, fresh frozen tissue sections of grade II and IV astrocytoma tumors in situ. (A) Confocal microscopic background corrected mean fluorescence intensity values of ErbB1 (▨) and integrin-β1 (□) receptors on grade II (*left*) and grade IV (*right*) astrocytoma tissue sections of brain tumors, removed during surgery and prepared for labeling as described in Material and Methods, are shown. (B) Acceptor bleaching FRET (abFRET) measurements were performed between ErbB1 and integrin-β1 on double-labeled astrocytoma sections (Cy3-528 for ErbB1 and Cy5-TS2 for integrin-β1) in the cases of all grade II (sample TC515; *upper series*) and grade IV (sample T82; *lower series*) astrocytoma tissue sections of brain tumors according to the technical steps detailed in Material and Methods. Of the investigated grade II and grade IV astrocytomas, representative fluorescence images of ErbB1 (*left*) and integrin-β1 (*middle*) expressions and the false color abFRET images (*right*) are shown. Intra-molecular abFRET efficiency between MHC-I and β_2-microglobulin was determined as positive reference control (14.1% ± 0.3%). (C) Summarized results of abFRET experiments on the investigated clinical, fresh frozen tissue sections of grade II (*left*) and grade IV (*right*) astrocytomas in situ. Of note, expression levels of both ErbB1 and integrin-β1 and their interaction were markedly higher in grade IV astrocytoma samples than in grade II tumors. (D) Elucidatory 3-dimensional correlation of ErbB1, integrin-β1 expression levels, and the corresponding ErbB1–integrin-β1 abFRET efficiencies in grade II (*yellow dots*) and grade IV (*red dots*) astrocytoma tissue sections. Note the clear separation of the cases by the abFRET efficiencies (*axis Z*).

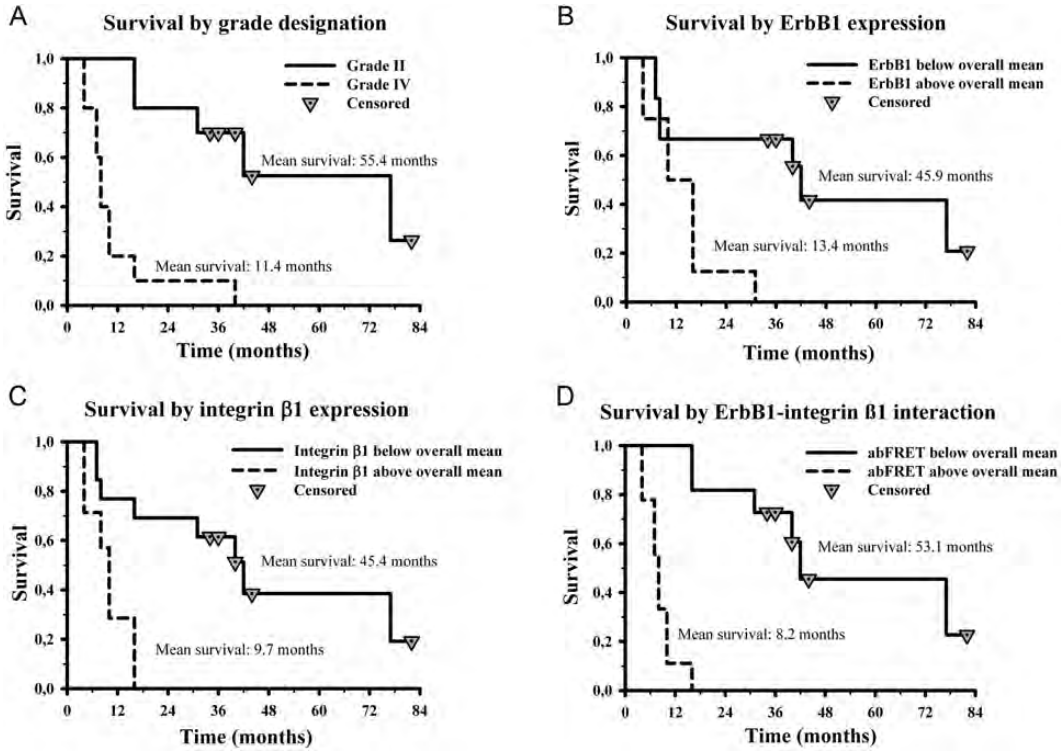

Fig. 5. Prognostic significance of ErbB1, integrin-β1 expression levels, and the degree of their heteroassociation in patients with astrocytic tumors. Overall survival, by grade designation (grade II and IV tumors), was determined using the Kaplan-Meier method (A). Survival among patients with tumors showing ErbB1 (B), integrin-β1 (C) expression levels, and abFRET efficiency states (D) below (——) or above (– – –) the overall mean were also compared. Statistical comparison of the indicated patient groups was estimated by the log-rank and post-hoc Holm-Sidak tests. Significance values are given as *P* values ($P < .001$, $P = .014$, $P = .004$, $P < .001$ for grade, ErbB1, integrin-β1, and the ErbB1–integrin-β1 heteroassociation, respectively).

modalities in select tumors, based on a proper understanding of the various signaling outcomes of specific molecular interactions. On the basis of our initial screen of receptor expression profiles in U251 glioblastoma subclones with extra chromosome 7 fragments, we analyzed the molecular interactions of ErbB1 and integrin-β1.

On U251 subclones, previously documented decreasing radiosensitivity[29] correlates with increasing ErbB1 expression levels. In addition to ErbB1, other molecules coded on chr. 7 that could contribute to decreased radiosensitivity are PMS2 (postmeiotic segregation increased 2), repairing mismatch DNS after radioinjury; MAD1 (mitotic arrest deficient-like 1), controlling mitotic assembly; and FAM126A (family with sequence similarity 126, member A), balancing the tumor-suppressing effect of the beta-catenin pathway. Our screen has shown that, parallel to the increase of ErbB1, the expression of integrin-β1 increased. Because integrin-β1 is not coded on chr. 7, its increased expression is likely to be the result of a regulatory pathway activated by excess ErbB1. To simplify the system in terms of additional expressed genes and to verify ErbB1-induced integrin-β1 upregulation, we stably transfected the ErbB1 gene into U251 cells, creating sublines with increased (E1L) and highly increased (E1H) ErbB1 expression.

In this system, ectopic ErbB1 also induced integrin-β1 overexpression and increased radioresistance. Of interest, integrin-β1 expression did not increase beyond a certain level, regardless of how much ectopic ErbB1 was in the cell membrane. Extremely high numbers of ErbB1 did not carry a selection advantage when the culture was passaged *en mass*, and the subpopulation (E1H/H) carrying these highly increased amounts of ErbB1 gradually disappeared. Contrary to this, the vast excess of ErbB1 in E1H provided a proliferative advantage in colony forming assay when the paracrine effects of denser cultures did not promote proliferation. Thus, it appears that surplus ErbB1 contributes primarily to colony forming ability even if it does not represent a proliferative advantage in regular cell cultures.

Excess integrin-β1 levels were equal and stable in the transfected subclones E1H and E1L, and there was no difference in radiation resistance between E1H and E1L. Both sublines showed a significant decrease of α in the linear-quadratic model of radiation resistance, compared with the mother cell line, indicating that cell proliferation became less sensitive to double-strand DNA breaks.

With regard to the signaling mechanisms that could contribute to the observed effects of excess ErbB1 and integrin-β1, the PI3K/Akt pathway has received much attention because of its negative regulation by the tyrosine phosphatase/tensin (PTEN) homolog protein, which most commonly has loss-of-function mutations in glioblastomas.[48] In addition to stimulating the STAT

transcription factors, this pathway was shown to modulate ErbB1-regulated activation of NF-kappa-β involved in transformation pathways.[49] More recently, radiation-induced Akt activation was proposed to modulate the radioresistance of human glioblastoma cells.[50] In our cellular models, an increased basal Akt phosphorylation and augmented output from the PI3K/Akt pathway after EGF stimulation was observed in the sublines with higher ErbB1 and integrin-β1 expression. Because PI3K inhibition reverses the radioresistance evoked in these sublines by the excess ErbB1 and integrin-β1 expression, the involvement of this pro-survival pathway in the increased radioresistance is plausible.

As for the molecular mechanism behind this shift of signaling emphasis, we show that there is an inverse correlation between ErbB1 homoassociation, higher in the mother cell line, and ErbB1–integrin-β1 heteroassociation, more dominant in the more radioresistant sublines. More specifically, this anticorrelation is not only substantiated on the level of population averages, but also on the submicron scale of membrane compartments, suggesting that excess integrin-β1 preferentially clusters with ErbB1, competitively diminishing the extent of interaction in ErbB1 homoclusters. The molecules involved in the synergism of the thereby evolving ErbB1–integrin-β1 molecular association are thought to be the focal adhesion kinase FAK, integrin-linked kinase ILK, and the bridging molecule PINCH.[51] In addition to Akt phosphorylation, similarly up-regulated pathways that may share functional relevance in vitro (as well as in vivo) could mainly be those related to adhesion and migration regulated by integrin signaling. Accordingly, the integrin-linked kinase/glycogen synthase kinase-3β (GSK-3β) mediated canonical β-catenin/Tcf-4 pathway was remarkably shown to not only be upregulated in astrocytomas but also bear direct regulating effect on Akt2 gene expression, thereby promoting glioma progression.[52] Ongoing preclinical studies now address PI3K-related pathway inhibitors (NVP-BEZ235, LY294002, enzastaurin) that suggest a potential to sensitize chemotherapy-induced apoptosis via disrupting the PI3K/Akt/mTOR (mammalian target of rapamycin)/GSK-3β signaling routes.[53]

With a view to expected clinical implications, we have developed a method to quantitate, in fresh frozen glioblastoma intraoperative samples, the actual extent of interaction between ErbB1 and integrin-β1. This approach shifts the information content from mere expression levels to a quasi-functional realm and affords the advantage of monitoring a reasonably stable molecular conformation relevant to an active signaling pathway. Comparing sets of grade II and grade IV tumors reveals that, coherent with the observation in our cellular model systems, increased integrin-β1 expression and ErbB1–integrin-β1 heteroassociation was more important in determining grade and outcome than were high ErbB1 levels. Survival time and time to relapse inversely correlated with in situ measurements of integrin-β1 expression and ErbB1–integrin-β1 heteroassociation. The latter as a single parameter served to classify tumor grade equally well as the complex histopathological diagnosis and was a single determinant of predicting outcome in stepwise multiple regression. In each group, there were extreme cases that diverged from the overall prognosis in the group, and although the small number of occurrences is not amenable to statistical analysis, stronger ErbB1–integrin-β1 interactions in each group predicted worse prognosis and vice versa.

On the basis of these results, elevated integrin-β1 expression and especially a high degree of ErbB1–integrin-β1 heteroassociation in astrocytic tumors could predict ineffective response to ionizing radiation and an unfavorable survival outlook, which could potentially be overcome by inhibiting the function of overexpressed proteins, their interactions, or the downstream output converging on the PI3K/Akt pathway. Determining integrin-β1 expression and ErbB1–integrin-β1 heteroassociation in newly diagnosed astrocytomas and/or quantitating the activation of relevant downstream effectors, such as PI3K, Akt, or GSK-3β, could allow for stratification into prognostically divergent patient subgroups and selection of appropriate therapeutic modalities.[54,55]

Supplementary Material

Supplementary material is available online at Neuro-Oncology (http://neuro-oncology.oxfordjournals.org/)

Funding

This work was supported by Hungarian National Research Fund OTKA (K75752, NK101337, F-049050), Hungarian Ministry of Health (ETT 523/2003, 362-01/2009), TÁMOP (4.2.1/B-09/1/KONV-2010-0007, 4.2.2/B-10/1/2010-0024, 4.2.2/A-11/1/KONV-2012-0025), and Baross Gábor Program (REG_EA_09-1-2009-0010).

Acknowledgments

We thank Ms. Gabriella Őri, Ms. Tünde Terdik, and Ms. Hajnalka Toldi, for their technical assistance, and Zsolt Fazekas and Mária Kern, for useful technical discussions.

Conflict of interest statement. None declared.

References

1. Dolecek TA, Propp JM, Stroup NE, Kruchko C. CBTRUS statistical report: primary brain and central nervous system tumors diagnosed in the United States in 2005-2009. *Neuro-oncology*. 2012;14(Suppl 5):v1-49.
2. National Cancer Institute. Surveillance, Epidemiology and End Results (SEER) Database: Surveillance, Epidemiology and End Results (SEER) Database.

3. National Comprehensive Cancer Network. Central Nervous System Cancers Practice Guidelines in Oncology. Vol 2. Jenkitown, PA2005.
4. Zhang H, Berezov A, Wang Q, et al. ErbB receptors: from oncogenes to targeted cancer therapies. *J Clin Invest*. 2007;117(8):2051–2058.
5. Sartor CI. Epidermal growth factor family receptors and inhibitors: radiation response modulators. *Semin Radiat Oncol*. 2003;13(1):22–30.
6. Schmidt-Ullrich RK, Contessa JN, Lammering G, Amorino G, Lin PS. ERBB receptor tyrosine kinases and cellular radiation responses. *Oncogene*. 2003;22(37):5855–5865.
7. Citri A, Yarden Y. EGF-ERBB signalling: towards the systems level. *Nat Rev Mol Cell Biol*. 2006;7(7):505–516.
8. Bowers G, Reardon D, Hewitt T, et al. The relative role of ErbB1–4 receptor tyrosine kinases in radiation signal transduction responses of human carcinoma cells. *Oncogene*. 2001;20(11):1388–1397.
9. Basson MD. An intracellular signal pathway that regulates cancer cell adhesion in response to extracellular forces. *Cancer Res*. 2008;68(1):2–4.
10. Brakebusch C, Bouvard D, Stanchi F, Sakai T, Fassler R. Integrins in invasive growth. *J Clin Invest*. 2002;109(8):999–1006.
11. Hehlgans S, Haase M, Cordes N. Signalling via integrins: implications for cell survival and anticancer strategies. *Biochim Biophys Acta*. 2007; 1775(1):163–180.
12. Mocanu MM, Fazekas Z, Petras M, et al. Associations of ErbB2, beta1-integrin and lipid rafts on Herceptin (Trastuzumab) resistant and sensitive tumor cell lines. *Cancer Lett*. 2005;227(2):201–212.
13. Huang J, Hu J, Bian X, et al. Transactivation of the epidermal growth factor receptor by formylpeptide receptor exacerbates the malignant behavior of human glioblastoma cells. *Cancer Res*. 2007;67(12):5906–5913.
14. Lee LT, Huang YT, Hwang JJ, et al. Transinactivation of the epidermal growth factor receptor tyrosine kinase and focal adhesion kinase phosphorylation by dietary flavonoids: effect on invasive potential of human carcinoma cells. *Biochem Pharmacol*. 2004;67(11):2103–2114.
15. Stommel JM, Kimmelman AC, Ying H, et al. Coactivation of receptor tyrosine kinases affects the response of tumor cells to targeted therapies. *Science*. 2007;318(5848):287–290.
16. Vereb G, Jr., Nagy P, Park JW, Szöllősi J. Signaling revealed by mapping molecular interactions: implications for ErbB-targeted cancer immunotherapies. *Clin Appl Immun Rev*. 2002;2:169–186.
17. Khwaja A, Rodriguez-Viciana P, Wennstrom S, Warne PH, Downward J. Matrix adhesion and Ras transformation both activate a phosphoinositide 3-OH kinase and protein kinase B/Akt cellular survival pathway. *Embo J*. 1997;16(10):2783–2793.
18. King WG, Mattaliano MD, Chan TO, Tsichlis PN, Brugge JS. Phosphatidylinositol 3-kinase is required for integrin-stimulated AKT and Raf-1/mitogen-activated protein kinase pathway activation. *Mol Cell Biol*. 1997;17(8):4406–4418.
19. Brunet A, Bonni A, Zigmond MJ, et al. Akt promotes cell survival by phosphorylating and inhibiting a Forkhead transcription factor. *Cell*. 1999;96(6):857–868.
20. Downward J. Mechanisms and consequences of activation of protein kinase B/Akt. *Curr Opin Cell Biol*. 1998;10(2):262–267.
21. Guo W, Giancotti FG. Integrin signalling during tumour progression. *Nat Rev Mol Cell Biol*. 2004;5(10):816–826.
22. Katz M, Amit I, Citri A, et al. A reciprocal tensin-3-cten switch mediates EGF-driven mammary cell migration. *Nat Cell Biol*. 2007;9(8):961–969.
23. Cordes N, Seidler J, Durzok R, Geinitz H, Brakebusch C. beta1-integrin-mediated signaling essentially contributes to cell survival after radiation-induced genotoxic injury. *Oncogene*. 2006;25(9): 1378–1390.
24. Park CC, Zhang HJ, Yao ES, Park CJ, Bissell MJ. Beta1 integrin inhibition dramatically enhances radiotherapy efficacy in human breast cancer xenografts. *Cancer Res*. 2008;68(11):4398–4405.
25. Mills JD, Stone JR, Rubin DG, et al. Illuminating protein interactions in tissue using confocal and two-photon excitation fluorescent resonance energy transfer microscopy. *J Biomed Opt*. 2003;8(3):347–356.
26. Schmid JA, Birbach A. Fluorescent proteins and fluorescence resonance energy transfer (FRET) as tools in signaling research. *Thromb Haemost*. 2007;97(3):378–384.
27. Kong A, Leboucher P, Leek R, et al. Prognostic value of an activation state marker for epidermal growth factor receptor in tissue microarrays of head and neck cancer. *Cancer Res*. 2006;66(5):2834–2843.
28. Konig P, Krasteva G, Tag C, Konig IR, Arens C, Kummer W. FRET-CLSM and double-labeling indirect immunofluorescence to detect close association of proteins in tissue sections. *Lab Invest*. 2006;86(8):853–864.
29. Misra A, Pellarin M, Hu L, et al. Chromosome transfer experiments link regions on chromosome 7 to radiation resistance in human glioblastoma multiforme. *Genes Chromosomes Cancer*. 2006;45(1):20–30.
30. Sebestyen Z, Nagy P, Horvath G, et al. Long wavelength fluorophores and cell-by-cell correction for autofluorescence significantly improves the accuracy of flow cytometric energy transfer measurements on a dual-laser benchtop flow cytometer. *Cytometry*. 2002;48(3): 124–135.
31. Szentesi G, Horvath G, Bori I, et al. Computer program for determining fluorescence resonance energy transfer efficiency from flow cytometric data on a cell-by-cell basis. *Comput Methods Programs Biomed*. 2004;75(3):201–211.
32. Jovin TM, Arndt-Jovin DJ. Luminescence digital imaging microscopy. *Annu Rev Biophys Biophys Chem*. 1989;18:271–308.
33. Szentesi G, Vereb G, Horvath G, et al. Computer program for analyzing donor photobleaching FRET image series. *Cytometry A*. 2005;67(2): 119–128.
34. Vereb G, Meyer CK, Jovin TM. Novel microscope-based approaches for the investigation of protein - protein interactions in signal transduction. In: Heilmeyer, MG, ed. Jr, Interacting protein domains, their role in signal and energy transduction. NATO ASI series. Vol H102. New York: Springer-Verlag; 1997:49–52.
35. Roszik J, Szollosi J, Vereb G. AccPbFRET: an ImageJ plugin for semi-automatic, fully corrected analysis of acceptor photobleaching FRET images. *BMC Bioinformatics*. 2008;9:346.
36. Fazekas Z, Petras M, Fabian A, et al. Two-sided fluorescence resonance energy transfer for assessing molecular interactions of up to three distinct species in confocal microscopy. *Cytometry A*. 2008; 73(3):209–219.
37. Sandfort V, Koch U, Cordes N. Cell adhesion-mediated radioresistance revisited. *Int J Radiat Biol*. 2007;83(11–12):727–732.
38. Friedlander DR, Zagzag D, Shiff B, et al. Migration of brain tumor cells on extracellular matrix proteins in vitro correlates with tumor type and grade and involves alphaV and beta1 integrins. *Cancer Res*. 1996;56(8): 1939–1947.
39. Westhoff MA, Zhou S, Bachem MG, Debatin KM, Fulda S. Identification of a novel switch in the dominant forms of cell adhesion-mediated drug resistance in glioblastoma cells. *Oncogene*. 2008; 27(39):5169–5181.
40. Abdollahi A, Griggs DW, Zieher H, et al. Inhibition of alpha(v)beta3 integrin survival signaling enhances antiangiogenic and antitumor effects of radiotherapy. *Clin Cancer Res*. 2005;11(17):6270–6279.

41. Eller JL, Longo SL, Kyle MM, Bassano D, Hicklin DJ, Canute GW. Anti-epidermal growth factor receptor monoclonal antibody cetuximab augments radiation effects in glioblastoma multiforme in vitro and in vivo. *Neurosurgery*. 2005;56(1):155–162. discussion 162.
42. Lomonaco SL, Finniss S, Xiang C, et al. Cilengitide induces autophagy-mediated cell death in glioma cells. *Neuro-oncology*. 2011;13(8): 857–865.
43. Kreisl TN, McNeill KA, Sul J, Iwamoto FM, Shih J, Fine HA. A phase I/II trial of vandetanib for patients with recurrent malignant glioma. *Neuro-oncology*. 2012;14(12):1519–1526.
44. Lee EQ, Kuhn J, Lamborn KR, et al. Phase I/II study of sorafenib in combination with temsirolimus for recurrent glioblastoma or gliosarcoma: North American Brain Tumor Consortium study 05–02. *Neuro-oncology*. 2012;14(12):1511–1518.
45. Razis E, Selviaridis P, Labropoulos S, et al. Phase II study of neoadjuvant imatinib in glioblastoma: evaluation of clinical and molecular effects of the treatment. *Clin Cancer Res*. 2009;15(19):6258–6266.
46. Nabors LB, Mikkelsen T, Rosenfeld SS, et al. Phase I and correlative biology study of cilengitide in patients with recurrent malignant glioma. *J Clin Oncol*. 2007;25(13):1651–1657.
47. Mikkelsen T, Brodie C, Finniss S, et al. Radiation sensitization of glioblastoma by cilengitide has unanticipated schedule-dependency. *Int J Cancer*. 2009;124(11):2719–2727.
48. Cantley LC, Neel BG. New insights into tumor suppression: PTEN suppresses tumor formation by restraining the phosphoinositide 3-kinase/AKT pathway. *Proc Natl Acad Sci USA*. 1999;96(8):4240–4245.
49. Kapoor GS, Zhan Y, Johnson GR, O'Rourke DM. Distinct domains in the SHP-2 phosphatase differentially regulate epidermal growth factor receptor/NF-kappaB activation through Gab1 in glioblastoma cells. *Mol Cell Biol*. 2004;24(2):823–836.
50. Li HF, Kim JS, Waldman T. Radiation-induced Akt activation modulates radioresistance in human glioblastoma cells. *Radiat Oncol*. 2009;4:43.
51. Qin J, Wu C. ILK: a pseudokinase in the center stage of cell-matrix adhesion and signaling. *Curr Opin Cell Biol*. 2012;24(5):607–613.
52. Zhang J, Huang K, Shi Z, et al. High beta-catenin/Tcf-4 activity confers glioma progression via direct regulation of AKT2 gene expression. *Neuro-oncology*. 2011;13(6):600–609.
53. Wick W, Weller M, Weiler M, Batchelor T, Yung AW, Platten M. Pathway inhibition: emerging molecular targets for treating glioblastoma. *Neuro-oncology*. 2011;13(6):566–579.
54. Sawyers CL. Cancer: mixing cocktails. *Nature*. 2007;449(7165): 993–996.
55. Wen PY, Lee EQ, Reardon DA, Ligon KL, Alfred Yung WK. Current clinical development of PI3K pathway inhibitors in glioblastoma. *Neuro-Oncology*. 2012;14(7):819–829.